Bioorganic & Medicinal Chemistry 20 (2012) 7206–7213

Contents lists available at SciVerse ScienceDirect

Bioorganic & Medicinal Chemistry

journal homepage: www.elsevier.com/locate/bmc

Bicyclic peptidomimetics targeting secreted aspartic protease 2 (SAP2) from *Candida albicans* reveal a constrained inhibitory chemotype

Chiara Calugi [a], Andrea Trabocchi [a,*], Flavia De Bernardis [b], Silvia Arancia [b], Pierluigi Navarra [d], Roberto Cauda [c], Antonio Cassone [b], Antonio Guarna [a,*]

[a] Department of Chemistry 'Ugo Schiff', University of Florence, Polo Scientifico e Tecnologico, Via della Lastruccia 13, 50019 Sesto Fiorentino, Florence, Italy
[b] Department of Infectious, Parasitic and Immune-mediated Diseases, Istituto Superiore di Sanità, Viale Regina Elena 299, 00161 Rome, Italy
[c] Department of Infectious Diseases, Catholic University of the Sacred Heart, Largo A. Gemelli 8, 00168 Rome, Italy
[d] Institute of Pharmacology, Catholic University of the Sacred Heart, Largo A. Gemelli 8, 00168 Rome, Italy

ARTICLE INFO

Article history:
Received 10 April 2012
Revised 6 September 2012
Accepted 11 September 2012
Available online 17 October 2012

Keywords:
Peptidomimetic
Infectious disease
Inhibitor
Protease
Molecular docking

ABSTRACT

The in vitro screening of stereoisomeric bicyclic peptidomimetics towards SAP2 of *Candida albicans* revealed a constrained chemotype as aspartic protease inhibitor in the micromolar to nanomolar range. The results indicated that the acetal bridge may serve as a transition-state isostere, and that the right match between interactions with subsites and the orientation by hydrogen bonding with Gly85 is the main requisite for inhibitory activity. Molecular docking calculations suggested the bicyclic acetal scaffold to be capable of interacting with the two catalytic aspartic acids, thus resulting in good inhibitory activity with only two hydrophobic groups addressing the enzyme catalytic subsites.

1. Introduction

The fungal pathogen *Candida albicans* is one of the leading causes of mucosal and systemic infections especially affecting immunodeficient individuals,[1] including those HIV-infected and patients undergoing cancer therapy.[2] When *Candida albicans* becomes pathogenic, it may cause a wide variety of infections ranging from mucosal to life threatening disseminated candidiasis.[3,4] In the last 50 years many antifungal drugs have been developed, but their intensive clinical use has favored the emergence of resistant strains,[5] thus highlighting the need of new molecules for drug-resistant fungal strains. New therapeutic approaches, such as those targeting virulence factors,[6] have been inspired from the success of new drugs targeting bacterial virulence in antimicrobial therapy.[7] *C. albicans* expresses ten distinct SAP (secreted aspartic protease) genes (SAP1-10) in vitro and in vivo.[8] Among them, SAP2 is one of the most expressed enzymes implicated in host invasion, it has been recognized as a crucial virulence factor for vaginal infection,[9] and both reversible and irreversible inhibitors have been reported, accordingly.[10] In 1999 the inhibition of proteases from *C. albicans* with HIV protease inhibitors was reported.[11] Moreover, structural data of SAP2 from *C. albicans* complexed with a potent inhibitor were reported,[12] and reversible transition-state-mimetic inhibitors,[13] such as **A-70450**, [10a,14] and also pseudo-irreversible inhibitors have been developed.[10b,c]

We recently identified a novel class of SAP2 peptidomimetic inhibitors based on the 6,8-dioxa-3-azabicyclo[3.2.1]octane scaffold.[15] Among this library of peptidomimetics the two hit candidates **1** and **3** (Fig. 1) proved to be effective against drug-resistant *C. albicans* strains in in vivo experiments. Such compounds are conceived as dipeptide isosteres, and the bicyclic acetal portion is attractive as a potential transition-state analogue in the interaction with key residues of enzyme's catalytic site. With aim to give insight into the binding mode of these compounds towards SAP2, we carried out a study by molecular modeling and enzyme inhibition assays, taking into account the four possible stereoisomers of the two lead compounds **1** and **3** (**2**, and **4**–**6**, respectively, Fig. 1). Moreover, we synthesized four possible stereoisomeric compounds containing leucine derivatives (compounds **7**–**10**, Fig. 1) in order to evaluate the effect of amino acid residues at the nitrogen atom of the bicyclic scaffold, and to study the topological requirements for inhibition of SAP2. Specifically, we arrayed the position and the stereochemistry of an amino acid side-chain isostere in the peptidomimetic scaffold by taking into account leucine as the probe amino acid.

* Corresponding authors. Tel.: +39 055 457 3507; fax: +39 055 457 3531 (A.T.); tel.: +39 055 457 3481; fax: +39 055 457 3569 (A.G.).
E-mail addresses: andrea.trabocchi@unifi.it (A. Trabocchi), antonio.guarna@unifi.it (A. Guarna).

0968-0896/$ - see front matter © 2012 Elsevier Ltd. All rights reserved.
http://dx.doi.org/10.1016/j.bmc.2012.09.031

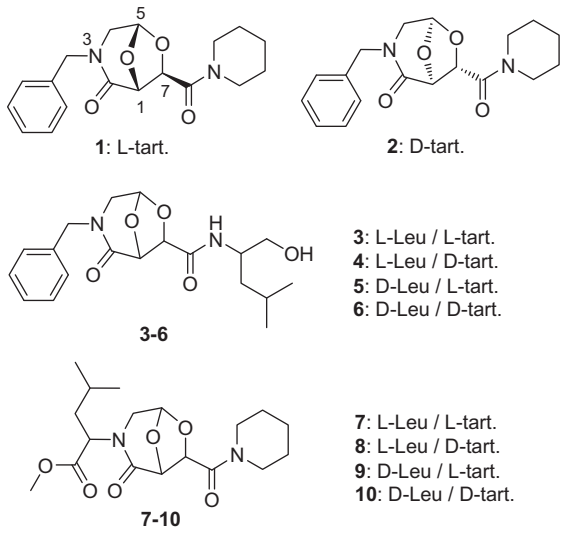

Figure 1. Stereoisomeric bicyclic peptidomimetics as SAP2 inhibitors.

2. Results and discussion

2.1. Synthesis

Compounds **7**–**10** were prepared using D- or L-leucine methyl ester as the starting material to build the bicyclic scaffold (Scheme 1).

As an exemplificative synthesis, compound **7** was obtained from L-leucine and L-tartaric acid derivatives. L-Leucine methyl ester hydrochloride [**(*S*)–I**] was subjected to reductive amination with dimethoxyacetaldehyde with catalytic Pd/C under a hydrogen atmosphere. The resulting amine [**(*S*)–II**] was converted into amide **III** through a coupling reaction with (2*R*,3*R*)-di-*O*-acetyl-tartaric anhydride, which was subsequently treated with thionyl chloride in MeOH to give the cyclic acetal **IV**. Then, trans-acetalization to give the bicyclic scaffold **V** was achieved in 66% overall yield by treating **IV** in refluxing toluene for 30 min, and in the presence of H_2SO_4 over silica gel. The target compound was finally achieved by heating methyl ester **V** in the presence of neat piperidine at 60 °C for 18 h, giving pure **7** in 65%, and in 43% overall yield accounting for the whole process.

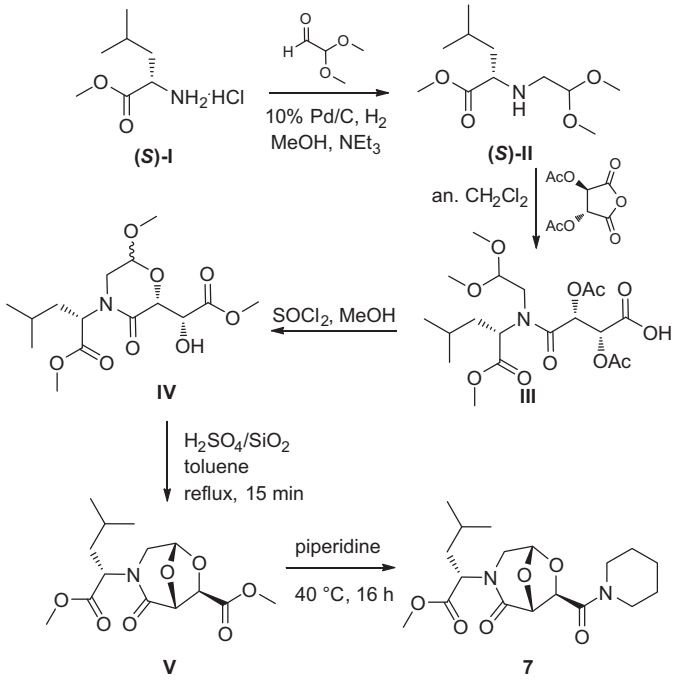

Scheme 1. Representative synthesis of leucine-derived compound **3**.

2.2. Enzyme inhibition assay

The screening of compounds **1**–**10** for enzyme inhibition was performed in order to evaluate the modulation of SAP2 inhibition by the stereochemical arrangement of pharmacophoric elements of the bicyclic peptidomimetics, and the different location of the amino acid side-chain isostere. The evaluation of protease activity inhibition was carried out by a spectrophotometric assay in comparison with pepstatin A as the reference inhibitor, and using 0.05% BSA as the substrate. Inhibition data (Table 1) showed compound **1** as the best inhibitor, possessing an IC_{50} of 30 nM. The corresponding enantiomer **2** inhibited SAP2 in the micromolar range, suggesting compound **1** to possess the correct stereochemistry and arrangement of the pharmacophoric groups.

Inhibition data of leucinol-derived compounds **3**–**6** showed the effect of substituting the piperidine at C-7 of the scaffold with an amino acid-derived moiety. The stereochemistry of the scaffold proved to play a minor role in this group of compounds, as both peptidomimetics **3** and **4** showed low micromolar activity, with the former displaying better inhibition capability. More importantly, loss of function was observed in parent compounds **5** and **6**, both having the leucinol moiety at C-7 with *R* absolute configuration at the stereogenic center, thus suggesting a mismatch irrespective of the stereochemistry of the bicyclic core. In the case of compounds **7**–**10**, possessing leucine and piperidino moieties at N-3 and C-7, respectively, reduced inhibition capacity towards SAP2 was observed only in the case of compound **8**, formally deriving from L-leucine and D-tartaric acid, as a consequence of a stereochemical configuration mismatch.

Thus, inhibition assay data suggested an adaptive behavior of the bicyclic peptidomimetic inhibitors in the catalytic site of SAP2 enzyme. This behavior may be accounted by the pseudosymmetric profile of the molecules, which allowed for orienting the two hydrophobic groups in two of the subsites flanking the catalytic site, irrespective of the stereochemistry of the scaffold. The mismatched configurations precluding inhibition activity were assessed in the case of compounds **5**, **6** and **8**, and optimal binding mode to SAP2 was found for compound **1**, which displayed nanomolar inhibition potency and an IC_{50} value three-times lower than the reference natural inhibitor pepstatin A (Table 1, entries 1 and 11).

2.3. Molecular modeling

Docking studies were performed with all the tested compounds showing a inhibition profile towards SAP2, in order to study the binding modes and their correlation with compounds stereochemistry. Autodock 4.0.1[16] was used to evaluate the binding energies of the selected conformations of compounds **1–4, 7** and **9–10** as SAP2 ligands. Best-scoring conformations of each ligand were clustered (Table 2) and visually inspected for enzyme–ligand interactions. Specifically, hydrogen bonds to side chain oxygen atoms of catalytic aspartic acids (Asp218 and Asp32), a double hydrogen-bond to the backbone nitrogen of Gly85 belonging to the 'flap region', and hydrophobic interactions in S1, S2, S1′ and S2′ pockets were taken into account. Moreover, the global minimum conformer of each molecule was subjected to a refinement within the enzyme catalytic site using the eMBrAcE minimization algorithm implemented in Macromodel.[17]

Table 1
Inhibition data for compounds **1**-**10** and pepstatin A

Compd	Structure	Precursor	IC_{50} (μM)
1	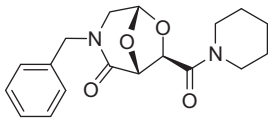	L-tart.	0.03
2	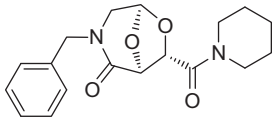	D-tart.	0.98
3	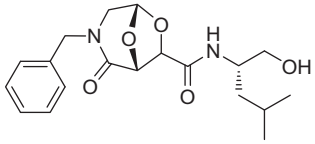	L-Tart. L-Leu	0.55
4	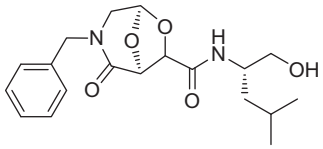	D-Tart. L-Leu	1.10
5	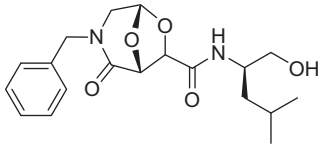	L-Tart. D-Leu	>10
6	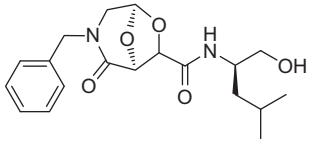	D-Tart. D-Leu	>10
7	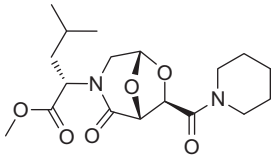	L-Tart. L-Leu	0.90
8	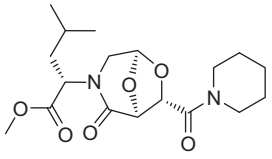	D-Tart. L-Leu	>10
9	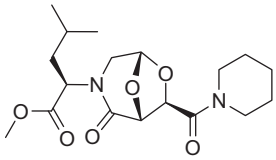	L-Tart. D-Leu	0.89
10	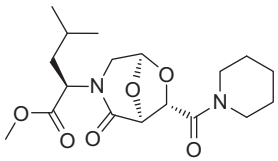	D-Tart. D-Leu	0.74
11	Pepstatin A		0.09

Docking results of **1–4** showed these inhibitors addressing S2, S2′ and S1 binding pockets, and the acetal bridge being oriented towards catalytic Asp32 and Asp218 (Fig. 2). Docking of **1** resulted in a main cluster of 36 out of 50 conformations characterized by a hydrogen-bond between the carbonyl group at position 2 of the scaffold and Gly85 amide proton (Fig. 2, top left), and by hydrophobic contacts with S2/S2′ binding pockets as the main interactions

Table 2
Cluster analysis for docking calculation of compounds **1**–**4**, **7** and **9**–**10**

Compd	Clusters[a]	Main cluster		
		Cluster members (out of 50 runs)	Lowest binding energy (kcal/mol)	Mean binding energy (kcal/mol)
1	6	36	−5.85	−5.73
2	8	28	−5.70	−5.51
3	22	10	−7.27	−6.53
4	25(12)[b]	9(35)	−5.53(−5.95)	−4.27(−5.15)
7	4	23	−5.69	−5.09
9	7	36	−5.81	−5.09
10	5	34	−5.36	−4.91

[a] Number of distinct conformational clusters out of 50 runs, using an rmsd of 2.0 A.
[b] In parentheses the number of distinct conformational clusters out of 100 runs and all the corresponding data.

for inhibition. Piperidino and benzyl moieties were observed in S2 and S2′ subsites, respectively. A edge-to-face interaction[18] between the benzyl group and Tyr84 side chain was observed as an additional hydrophobic contact. The eMBrAcE minimization of the enzyme-inhibitor complex confirmed the arrangement found in the docking calculation. The importance of the hydrogen-bond with Gly85 was in agreement with the key role of such amino acid as the anchoring point in SAP2 active site, as also reported in the literature for the inhibitor **A-70450**. [10a] Moreover, the orientation of the acetal bridge in the catalytic site suggested its possible role as a transition-state isostere.

The main cluster of **2** (Fig. 2, top right) showed a similar binding profile as for **1**, although lacking the key hydrogen-bond with Gly85. The benzyl group was found in the S2′ subsite, showing a edge-to-face interaction with Tyr84 as for **1**, and the piperidino moiety in the S2 cavity. The eMBrAcE minimization of the enzyme-inhibitor complex confirmed such reversed arrangement found in the docking calculation. This result indicated that the establishment of hydrophobic contacts is important for the molecular recognition in the catalytic site, accounting for an inhibition potency in the micromolar range, and that a hydrogen-bond with Gly85 amide proton is crucial in assessing a tight binding interaction between the protease and the peptidomimetic, in agreement with inhibition data of **1** as compared to **2** (Table 1).[19]

Compound **3** displayed an interesting reversed orientation of the substituents in the binding site with respect to **1**, as confirmed by the eMBrAcE minimization of the enzyme-inhibitor complex. Although this calculation did not converge as other compounds (see Table 2 for the cluster analysis), the main cluster of conformations showed the benzyl group being placed in the S1 subsite, the isobutyl group of the leucinol moiety in the S2′ pocket, and the hydroxyl group arranged in the S1′ subsite (Fig. 2, bottom left). In this reversed arrangement the orientation of the acetal bridge facing the catalytic aspartic acid residues was preserved, but not the interaction with the Gly85. Specifically, the hydroxyl group of **3** established a hydrogen-bond with Glu193 side-chain, and the amide proton of **3** with Gly34 carbonyl group. Moreover, a π–π stacking-type interaction was observed between the benzyl group and Tyr84 side chain. Thus, a different functionalization at position 7 of the same scaffold as of **1** produced a diverse binding mode in the enzyme catalytic site, although in the micromolar range (Table 1).

The docking analysis of **4** resulted in a large cluster family as of **3**, and the simulation using 100 runs allowed for improving the quality of the calculation by halving the number of clusters from 25 to 12 (Table 2). The low-energy cluster of conformations from docking of **4** did not show a reversed orientation of the substituents in the binding pockets as for **3**. Specifically, the benzyl group

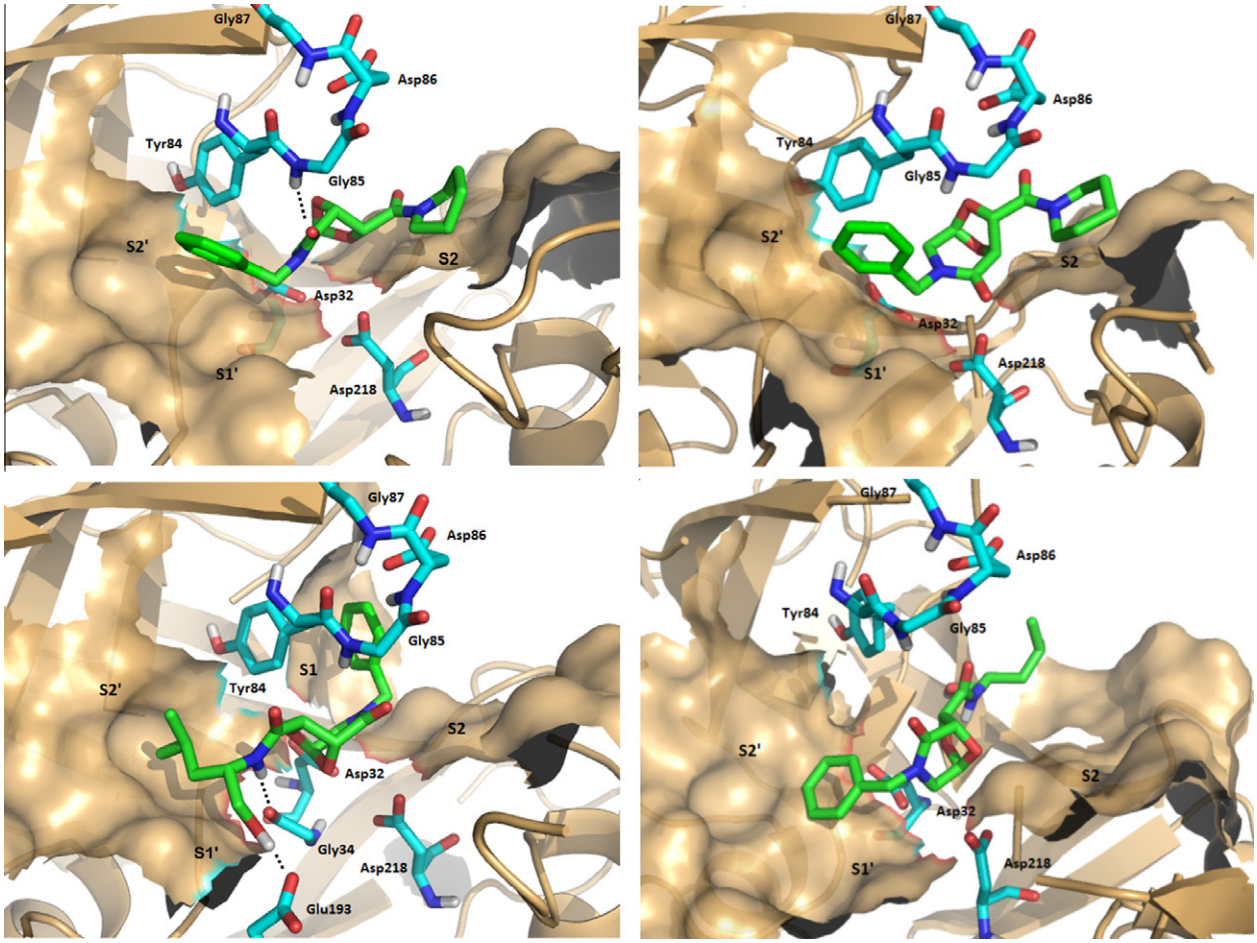

Figure 2. Best-scoring docked conformations resulting from the docking of hit compounds **1** (top left), **2** (top right), **3** (bottom left) and **4** (bottom right).

was found in the S2′ subsite, and the isobutyl moiety in S1. As for **1**, the carbonyl group at position 2 of the bicyclic scaffold interacted through a hydrogen-bond with Gly85, although showing a greater distance between C=O and NH groups. Even if possessing such key hydrogen-bond as for **1**, the micromolar activity could be explained using the eMBrAcE minimization of the enzyme-inhibitor complex. Indeed, the low-energy conformation found in the calculation did not display the typical stabilizing interactions as above (Fig. 2, bottom right). This was in agreement with the lower inhibitory profile of **4** with respect to the stereoisomeric compound **3**.

Docking simulations of compounds **5** and **6** did not converge to any specific cluster of conformations, but produced an array of different solutions. This result was in agreement with enzyme inhibition data indicating no activity at 10 μM concentration.

As regarding to stereoisomeric leucine-derived compounds **7**–**10**, no significant differences between the binding modes of stereoisomers **7** and **9** were found, whereas **10** resulted in a reversed orientation as for **3**, and docking calculations of compound **8**, deriving from L-leucine and D-tartaric acid, did not produce a low-energy cluster of solutions. All docking simulations of the three stereoisomers resulted in lower-energy clusters of conformations showing a common interaction motif between the bicyclic scaffold and Gly85 as the most important polar interaction. Moreover, compound **7** showed an additional hydrogen-bond to Gly85 with the carbonyl function of the leucine derivative. [10a]

Compound **7** showed an orientation in the active site similar to compound **1**. In fact, the piperidino group was found in the S2 subsite, the methyl ester in proximity of S2′, and the isobutyl moiety deriving from leucine was in the S1′ subsite (Fig. 3, top). Nevertheless, a higher distance to catalytic aspartic acid residues was observed, possibly explaining the reduced inhibition profile with respect to **1**. The deeper and narrower cavity around the S2′ subsite clearly indicated the methyl group of **7** to be inadequate for establishing a strong hydrophobic contact, and suggesting a possible improvement of the potency by placing a longer aliphatic chain at such position.

The main cluster of conformations of compound **9** showed a similar binding profile as for compound **7**, although lacking the additional hydrogen-bond between Gly85 and the methyl ester's carbonyl group (Fig. 3, center). Indeed, the isobutyl moiety was found to occupy the S2′ pocket, whereas the ester group was positioned in the S1′ subsite in a reversed arrangement with respect to **7**. Compound **10** (Fig. 3, bottom) showed a reversed orientation as found for **3**, thus corroborating the hypothesis of an adaptive behaviour of this class of bicyclic peptidomimetic inhibitors. Moreover, the interaction of the piperidino group with the S2 subsite confirmed the key hydrophobic interaction with such cavity, and the stereochemistry L-leucine moiety at N-3 of the D-tartaric acid-derived scaffold as the matched configuration for interacting with the flat S2′ subsite.

The crystal structure of **A-70450** (K_i = 12 nM) [10a] complexed with SAP2 provides evidence on the typical binding interactions with the enzyme active site (PDB code: 1EAG).[20] Thus, the structural alignment of selected backbone atoms of peptidomimetics

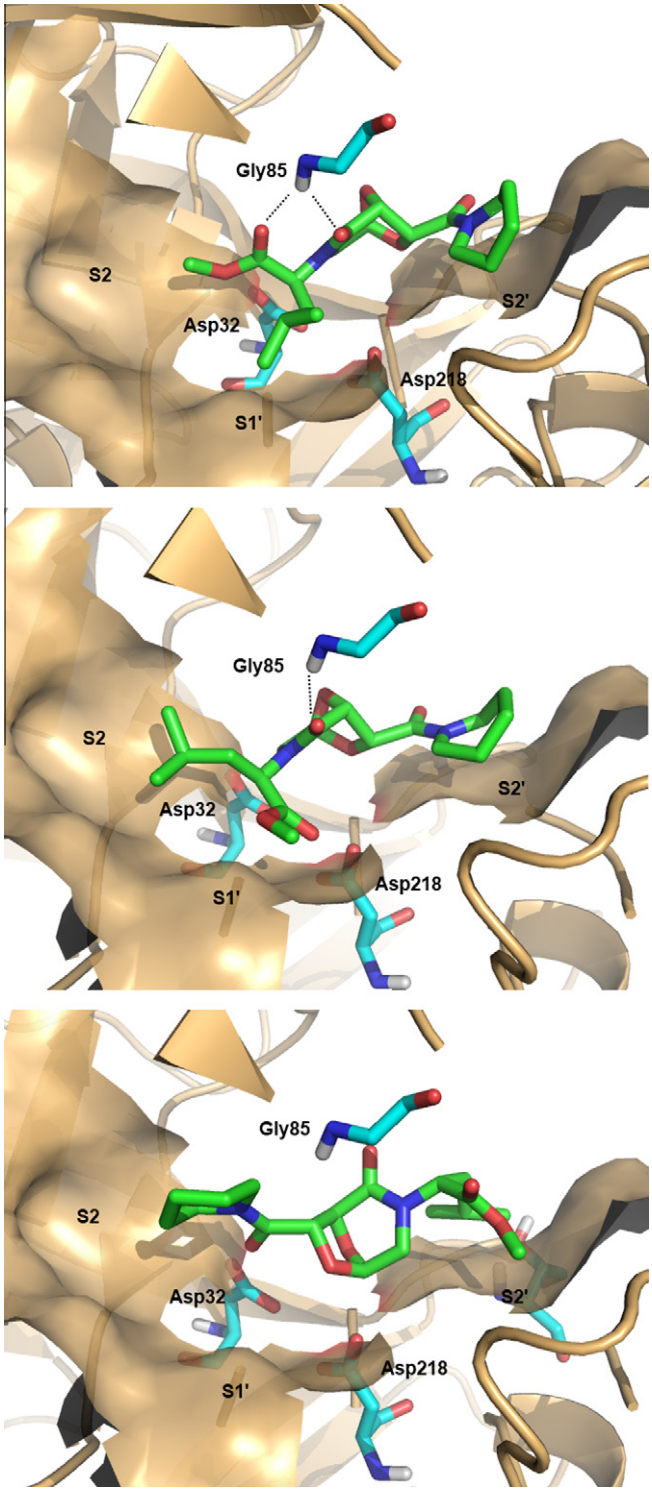

Figure 3. Best-scoring docked conformations resulting from the docking of compounds **7**–**10**: **7**, top; **9**, center; **10**, bottom. The protein residues that form key interactions are highlighted in cyan. Non-polar hydrogen atoms are omitted for clarity.

in their docked conformation with respect to the bioactive conformation of **A-70450** was carried out to gain further insight into the binding mode of the bicyclic peptidomimetics towards SAP2. According to docking calculations, three-to-four backbone atoms of the peptidomimetics were taken into account for the overlay with **A-70450** (Fig. 4), and RMSD was calculated as measure of

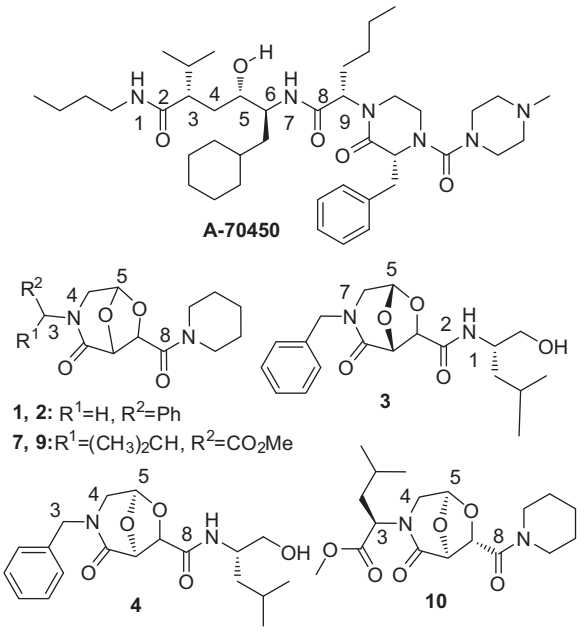

Figure 4. Selected backbone atoms of peptidomimetics and **A-70450** for the structural alignment.

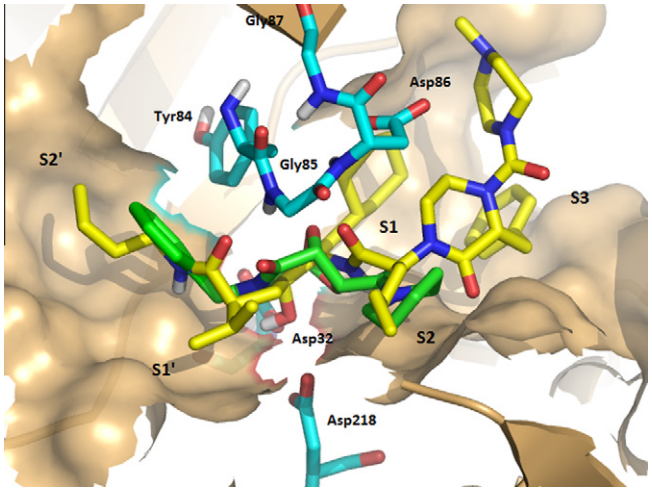

Figure 5. Overlap of best-scoring conformation resulting from the docking of **1** (green) and reference SAP2 inhibitor **A-70450** (yellow). Key protein residues are highlighted in cyan. Non-polar hydrogen atoms are omitted for clarity.

Table 3
[a]RMSD deriving from the structural alignment of selected backbone atoms of peptidomimetics in their docked conformation with respect to the bioactive conformation of **A-70450**.

Compd	RMSD (3 atoms)	RMSD (4 atoms)
1	0.59	0.64
2	0.61	0.64
3	0.37	0.43
4	0.63	0.65
7	0.61	0.68
9	0.60	0.67
10	0.60	0.64

[a] The RMS deviation is reported in ang, and is referred to the atom positions of the inhibitors with respect to those of the reference structure **A-70450** in the bioactive conformation (see Supplementary data for visual presentations of molecular overlays).

overlapping degree. The docked conformation of **1** overlapped nicely with **A-70450** with an RMSD value of 0.64 over 4-atoms overlay, and showed a similar orientation of the two butyl groups of **A-70450** and the substituents of **1** (Fig. 5 and Supplementary data). Specifically, the benzyl group of **1** addressed the S2′ pocket as for the butyl moiety of **A-70450**, whereas the piperidino group was found in the S2 subsite similarly to the butyl chain of **A-70450**. The acetal bridge overlapped the hydroxyl group interacting with Asp32 and Asp218, thus confirming the hypothesis of the role of such group as a transition-state isostere. Finally, the carbonyl group at C-2 of the scaffold displayed the key hydrogen-bond with Gly85 amide proton, in analogy with such interaction observed between **A-70450** and SAP2. [10a]

As for the other compounds as shown in Figure 4, the adaptive behavior observed in docking calculations was confirmed in molecular overlays, too. The superimposition of **A-70450** with the low-energy docked conformations of **7** showed a similar profile with respect to the orientation of P2 and P2′ pharmacophoric groups of **A-70450** and the ligand's substituents. In particular, the carbonyl moiety belonging to the leucine moiety displayed the same orientation of one of the **A-70450** carbonyl groups in establishing the key hydrogen-bond with Gly85, and the isobutyl side chain addressed the same S1′ pocket as for the **A-70450** isopropyl moiety. The inverse binding mode of **3** with respect to **1** resulted in a similar overlay profile (Table 3) of the piperidino and leucinol side-chain groups with respect to **A-70450** butyl groups, and being inverted with respect to **1**. The carbonyl groups at positions 2 and 8 of **A-70450** (Fig. 4) overlapped nicely with those of **3**, and so as for the acetal portion with respect to the hydroxyl moiety of the reference inhibitor.

3. Conclusion

In conclusion, we reported a detailed binding mode analysis of a series of bicyclic peptidomimetics possessing micromolar to nanomolar inhibition towards SAP2 of *C. albicans*. Enzyme inhibition assays suggested compound **1** as the most potent SAP2 inhibitor of the series. Micromolar activity was observed for compounds **2**–**4**, whereas no inhibition was found for (*R*)-leucinol-derived compounds **5** and **6**, indicating the detrimental effect of such stereochemical configuration towards inhibition. Enzyme inhibition assays of stereoisomeric leucine-derived compounds **7**–**10** indicated an inhibitory activity similar to the other leucine-derived hit compounds **2**–**4**, suggesting the adaptive behavior of these peptidomimetics in addressing the two subsites flanking the catalytic aspartic acid residues. Only in the case of compound **8**, formally deriving from L-leucine and D-tartaric acid, the inhibition potency was impaired as a consequence of a mismatched stereochemical configuration. Molecular modeling calculations confirmed the hypothesized adaptive behavior of the bicyclic compounds in orienting the pharmacophoric groups in SAP2 catalytic site, and showed hydrophobic contacts to S2/S2′/S1′ and hydrogen-bonding interactions to Gly85 as the main elements for inhibition.

Finally, a putative role of the acetal bridge as a transition-state isostere interacting with catalytic Asp32 and Asp218 was assumed, as in all the clusters the acetal portion was found facing the aspartate residues. All favorable interactions were matched only by **1**, which showed nanomolar inhibition towards SAP2. The binding requirements for inhibition as observed in this study may help in designing new inhibitors taking advantage of Gly85 as the key anchoring site, which is found in the flap region opposite to catalytic Asp32 and Asp218. Finally, the introduction of bicyclic acetals as novel elements for interacting with catalytic aspartic acid residues suggests this moiety as a promising element in the design of new aspartic protease inhibitors.

4. Experimental section

4.1. General

Chromatographic separations were performed over silica gel (Kieselgel 60, Merck) using flash-column techniques; R_f values refer to TLC carried out on 25-mm silica gel plates (Merck F_{254}) with the same eluant as indicated for column chromatography. ^{1}H NMR spectra were recorded with Varian Gemini NMR spectrometers operating at 200 MHz for the proton and 50 MHz for the carbon. ESI mass spectra were carried out on an ion-trap double quadrupole mass spectrometer using electrospray (ES^+) ionization techniques, and a normalized collision energy within the range of 21–28 eV for MSMS experiments. Compounds **1**–**6** were prepared as reported.[15]

4.2. (*S*)-Methyl 2-(2,2-dimethoxyethylamino)-4-methylpentanoate [(*S*)-II]

A methanolic solution containing L-leucine methyl ester hydrochloride (6.9 g, 38 mmol), aqueous 60% dimethoxy acetaldehyde (5.7 mL, 6.59 g, 38 mmol), triethylamine (5.3 mL, 3.84 g, 38 mmol) and 10% Pd/C (552 mg) was stirred under a H_2 atmosphere and at room temperature for 16 h. The reaction mixture was then filtered over celite and concentrated under reduced pressure. The crude product was purified by flash chromatography (silica gel, EtOAc/petr. et. 1:2 + 1‰ Et_3N) affording the title compound as a yellow oil (4.90 g, 55% yield). $[\alpha]_D^{24}$ −22.9 (*c* 1.0, $CHCl_3$). ^{1}H NMR (200 MHz, $CDCl_3$) δ 4.43 (dd, *J* = 6.2, 4.8 Hz, 1 H), 3.70 (s, 3H), 3.35 (s, 3H), 3.34 (s, 3H), 3.30 (m, 1H), 2.73 (dd, *J* = 11.7, 6.2 Hz, 1H), 2.56 (dd, *J* = 11.7, 4.7 Hz, 1H), 1.71 (m, 2H), 1.46 (m, 2H), 0.89 (d, *J* = 4.4 Hz, 3H), 0.87 (d, *J* = 4.4 Hz, 3H). ^{13}C NMR (200 MHz, $CDCl_3$) δ 175.8 (s), 103.8 (d), 60.0 (d), 54.2 (q), 53.3 (q), 52.0 (q), 49.5 (t), 42.8 (t), 25.4 (d), 22.5 (q), 22.2 (q). ESI-MS: (*m*/*z*) 233.2 [M^++H, 23], 202.3 [100], 158.2 [43].

4.3. (*R*)-Methyl 2-(2,2-dimethoxyethylamino)-4-methylpentanoate [(*R*)-II]

Compound **(*R*)-II** was prepared as reported for **(*S*)-II** starting from D-leucine methyl ester hydrochloride (1.38 g, 7.6 mmol). After chromatographic purification, pure **(*R*)-II** (1.01 g, 4.33 mmol) was obtained in 57% yield with same characterization data as for **(*S*)-II**. $[\alpha]_D^{24}$ 23.3 (*c* 0.7, $CHCl_3$).

4.4. (*S*)-Methyl 4-methyl-2-((1*R*,5*R*,7*R*)-2-oxo-7-(piperidine-1-carbonyl)-6,8-dioxa-3-azabicyclo[3.2.1]octan-3-yl)pentanoate (7)

To a suspension of (2*R*,3*R*)-2,3-di-*O*-acetyl-tartaric anhydride (2.2 g, 10 mmol) in dry CH_2Cl_2 (7 mL) was added, at 0 °C and under a nitrogen atmosphere, a solution of **(*S*)-II** (2.50 g, 10 mmol) in dry CH_2Cl_2 (7 mL). The reaction was stirred at room temperature for 5 h. After evaporation of the solvent under reduced pressure, the crude adduct **III** was dissolved in MeOH (21 mL) and thionyl chloride (506 μL, 7 mmol) was added dropwise at 0 °C. The reaction mixture was stirred at room temperature for 16 h. Then, the reaction mixture was concentrated, diluted with CH_2Cl_2 and washed with 5% $NaHCO_3$ solution and brine. The organic layer was dried over Na_2SO_4 and evaporated. The crude product, isolated as an orange oil, was used in the next step without further purification. Specifically, a solution of the acetal **IV** (3.02 g, 9 mmol) was dissolved in a toluene-CH_2Cl_2 mixture (7 mL and 2 mL, respectively) and quickly added to a refluxing suspension of SiO_2/H_2SO_4 in toluene (8 mL). The mixture was allowed to react for 15 min,

then 1/4 of the solvent was distilled off. The hot reaction mixture was filtered through a $NaHCO_3$ pad and concentrated under reduced pressure. The crude product was purified by flash chromatography (silica gel, EtOAc/petr. et. 3:2, R_f = 0.30) to afford the corresponding bicyclic ester **V** as an orange solid (1.8 g, 66% yield over three steps). Compound **V** (1.8 g, 6 mmol) was dissolved in piperidine (6 ml, 5.11 g, 60 mmol) and the reaction mixture was allowed to reach 40 °C and stirred overnight. Then, the reaction mixture was diluted with CH_2Cl_2 and washed with a solution of 5% HCl and brine. The aqueous layer was extracted with CH_2Cl_2. The organic layer dried over Na_2SO_4 and concentrated under reduced pressure. The crude product was purified by flash chromatography (silica gel, EtOAc/petr. et. 3:2, R_f 0.31) to give pure **7** as a white solid (1.38 g, 65% yield, 43% overall yield). $[\alpha]_D^{24}$ −73.7 (*c* 1.0, $CHCl_3$), ^{1}H NMR (200 MHz, $CDCl_3$) δ 5.85 (d, *J* = 2.2 Hz, 1H), 5.17 (m, 1H), 5.09 (s, 1H), 4.89 (s, 1H), 3.68 (s, 3H), 3.62–3.44 (m, 3H), 3.35 (dd, *J* = 11.3, 2.2 Hz, 1H), 3.23 (d, *J* = 11.3 Hz, 1H), 1.68–1.58 (m, 10H), 0.93–0.87 (m, 6H). ^{13}C NMR (200 MHz, $CDCl_3$) δ 171.2 (s), 167.6 (s),165.0 (s), 99.5 (d), 78.0 (d), 76.4 (d), 52.2 (d), 47.7 (q), 46.5 (t), 43.5 (t), 35.9 (t), 26.4 (d), 25.5 (t), 24.7 (t), 23.3 (q), 21.2 (q). ESI-MSMS: (*m*/*z*) 369.1 [M^++H, 26], 336.9 [52], 309.2 [100], 256 [27].

4.5. (*S*)-Methyl 4-methyl-2-[(1*S*,5*S*,7*S*)-2-oxo-7-(piperidine-1-carbonyl)-6,8-dioxa-3-azabicyclo[3.2.1]octan-3-yl)]pentanoate (8)

Compound **8** was prepared as reported for **7** starting from (2*S*,3*S*)-2,3-di-*O*-acetyl-tartaric anhydride (2,6 g, 11.8 mmol and **(*S*)-II** (2.95 g, 11.8 mmol). After chromatographic purification, pure **8** (1.87 g, 5.07 mmol) was obtained in 43% yield. $[\alpha]_D^{24}$ −23.6 (*c* 1.0 $CHCl_3$), ^{1}H NMR (200 MHz, $CDCl_3$) δ 5.84 (d, *J* = 2.2 Hz, 1H), 5.07 (s, 1H), 5.05 (m, 1H), 4.77 (s, 1H), 3.67 (s, 3H), 3.51 (dd, *J* = 11.7, 2.2 Hz, 1H), 3.46–3.38 (m, 3H), 3.14 (d, *J* = 11.7 Hz, 1H), 1.72–1.42 (m, 10 H), 0.90 (m, 6H). ^{13}C NMR (200 MHz, $CDCl_3$) δ 170.8 (s), 166.8 (s),164.8 (s), 99.6 (d), 78.0 (d), 76.5 (d), 52.4 (d), 48.6 (q), 46.4 (t), 43.5 (t), 36.8 (t), 26.4 (d), 25.5 (t), 24.8 (t), 23.2 (q), 21.5 (q). ESI-MSMS: (*m*/*z*) 369.0 [M^++H, 4], 337.0 [100], 309.0 [53], 256 [3].

4.6. (*R*)-Methyl 4-methyl-2-[(1*R*,5*R*,7*R*)-2-oxo-7-(piperidine-1-carbonyl)-6,8-dioxa-3-azabicyclo[3.2.1]octan-3-yl]pentanoate (9)

Compound **9** was prepared as reported for **7** starting from (2*R*,3*R*)-2,3-di-*O*-acetyl-tartaric anhydride (2.20 g, 10 mmol and **(*R*)-II** (2.50 g, 10 mmol). After chromatographic purification, pure **9** (1.30 g, 3.54 mmol) was obtained in 40% yield with same characterization data as for **8**. $[\alpha]_D^{24}$ −28.3 (*c* 1.0 $CHCl_3$).

4.7. (*R*)-Methyl 4-methyl-2-((1*S*,5*S*,7*S*)-2-oxo-7-(piperidine-1-carbonyl)-6,8-dioxa-3-azabicyclo[3.2.1]octan-3-yl)pentanoate (10)

Compound **10** was prepared as reported for **7** starting from (2*S*,3*S*)-2,3-di-*O*-acetyl-tartaric anhydride (2,2 g, 10 mmol and **(*R*)-II** (2.50 g, 10 mmol). After chromatographic purification, pure **10** (1.40 g, 3.80 mmol) was obtained in 66% yield with same characterization data as for **7**. $[\alpha]_D^{24}$ 76.2 (*c* 1.0, $CHCl_3$).

4.8. Enzyme inhibition assay

Spectrophotometric method: the inhibition of protease activity by compounds **1**–**10** was measured by a spectrophotometric assay in comparison with pepstatin A activity, at the same concentration. Each assay contained 50 μL of the sample in 0.4 mL of 0.05% (w/v) bovine serum albumin (BSA) in 50 mM sodium citrate, pH 3.2, and 50 μL of protease solution (1 μg/mL) After 30 min at 37 °C, 1 mL of 10% (w/v) trichloroacetic acid was added. The tubes were stored in ice for 30 min, and then centrifuged (3000 g) for 10 min. The absorbance of the supernatant was read at 280 nm, using 0.05% BSA in citrate buffer as the control. One unit of the enzyme catalyzed a ΔA_{280} of 1 min^{-1}. With the pure protease the assay was proportional to enzyme concentration over the range ΔA_{280} 0.1–0.4 and a limit detection of 1 μg.[21] The difference of optical density (ΔOD) of 1 mL of solution in 1 minute was determined at different concentrations (5, 1, 0.1 μM, 5, 1 and 0.1 nM) of the inhibitors. For all data corresponding to in vitro experiments the standard deviation (SD) value was never above 5%. The IC_{50} values were determined by fitting binding inhibition data by non-linear regression using GraphPad Prism 4.0 Software Package (GraphPad Prism, San Diego, CA).

4.9. Molecular docking calculations

Automated docking studies were performed using the AutoDock 4.0.1 program,[16] an automated docking suite that employs a Lamarckian genetic algorithm (LGA) as the search engine. The Autodocktools 1.4.5 (ADT) graphical interface was used to prepare the enzyme and the PDBQT files of the ligands.[22] The 3D structures of the ligands were generated using Spartan (version 5.147), and then energy-minimized with the same program. The equilibrium geometry was calculated through the AM1 semi-empirical method. The coordinates of SAP2 were retrieved from the Protein Data Bank (PDB code: 1EAG). The ligand-protein complex was unmerged for achieving the free enzyme structure and water molecules were removed. Hydrogens were added to the enzyme and the ligands, Gasteiger charges were computed and non-polar hydrogens were merged. Three-dimensional energy scoring grids of 0.375 Å resolution and 40 Å × 40 Å × 40 Å or 64 Å × 64 Å × 64 Å dimensions were computed. The center of the grid was set on the side-chain carbon of Asp 218. Each docking experiment was derived from a total of 50 runs with a maximum of 2.5×10^6 energy evaluations, and using the default parameters for LGA. The cluster analysis was performed on the docked results using a root-mean-square deviation (rmsd) of 2.0 Å. The binding mode analyses of the docked conformations were carried out using PyMol Autodock Tools plugin within PyMol software.[23] The obtained docked target-ligand complexes were optimized with Macromodel[17] by the eMBracE energy minimization algorithm. The embrace minimization was carried out using Polak–Ribier conjugate gradient (PRCG). The optimizations were converged to a RMS energy gradient less than 0.05 KJ mol^{-1}, or continued until a limit of 1.000 iterations was reached. The force field used was OPLSA*,[24] with the water GB/SA solvent treatment at a dielectric constant of 1.0.[25] Normal cutoff distances were defined at 7 Å for van der Walls, 12 Å for electrostatics and 4 Å for hydrogen-bonds. The structural overlays between selected peptidomimetics and **A-70450,** and the corresponding rmsd calculations were obtained by using the Maestro graphical interface (Schrödinger, inc).

Acknowledgments

The financial support received from the Fondazione Roma, MIUR, Università degli Studi di Firenze, CINMPIS, Istituto Superiore di Sanità, and Programma Nazionale AIDS (Ministero della Salute-Istituto Superiore di Sanità) is gratefully acknowledged.

Supplementary data

Supplementary data associated with this article can be found, in the online version, at http://dx.doi.org/10.1016/j.bmc.2012.09.031.

References and notes

1. Marr, K. A. *Curr. Opin. Oncol.* **2009**, *22*, 138.
2. (a) Pfaller, M. A.; Diekema, D. J. *Clin. Microbiol. Rev.* **2007**, *20*, 133; (b) Wisplinghoff, H.; Bischoff, T.; Tallent, S. M.; Seifert, H.; Wenzel, R. P.; Edmond, M. B. *Clin. Infect. Dis.* **2004**, *39*, 309; (c) Sims, C. R.; Ostrosky-Zeichner, L.; Rex, J. H. *Arch. Med. Res.* **2005**, *36*, 660.
3. Mishra, N. N.; Prasad, T.; Sharma, N.; Payasi, A.; Prasad, R.; Gupta, D. K.; Singh, R. *Acta Microbiol. Immunol. Hung.* **2007**, *54*, 201.
4. (a) Hube, B. *Curr. Opin. Microbiol.* **2004**, *7*, 336; (b) Calderone, R. A.; Fonzi, W. A. *Trends microbiol.* **2001**, *9*, 327.
5. Akins, R. A. *Med. Mycol.* **2005**, *43*, 285.
6. Gauwerky, K.; Borelli, C.; Korting, H. C. *Drug Discovery Today* **2009**, *14*, 214.
7. (a) Alksne, L. E.; Projan, S. J. *Curr. Opin. Biotechnol.* **2000**, *11*, 625; (b) Alekshun, M. N.; Levy, S. B. *Drug. Discovery Today: Ther. Strateg.* **2004**, *1*, 483; (c) Naglik, J. R.; Challacombe, S. J.; Hube, B. *Microbiol. Mol. Biol. Rev.* **2003**, *67*, 400.
8. (a) Ollert, M. W.; Wende, C.; Görlich, M.; McMullan-Vogel, C. G.; Borg-von Zepelin, M.; Vogel, C. W.; Korting, H. C. *J. Clin. Microbiol.* **1995**, *33*, 2543; (b) Wu, T.; Wright, K.; Hurst, S. F.; Morrison, C. J. *Antimicrob. Agents Chemother.* **2000**, *44*, 1200; (c) Navarathna, D. H.; Hornby, J. M.; Hoerrmann, N.; Parkhurst, A. M.; Duhamel, G. E.; Nickerson, K. W. *J. Antimicrob. Chemother.* **2005**, *56*, 1156.
9. Cassone, A.; De Bernardis, F.; Mondello, F.; Ceddia, T.; Agatensi, L. *J. Infect. Dis.* **1987**, *156*, 777.
10. (a) Pranav Kumar, S. K.; Kulkarni, V. M. *Bioorg. Med. Chem.* **2002**, *10*, 1153; (b) Degel, B.; Staib, P.; Rohrer, S.; Scheiber, J.; Martina, E.; Büchold, C.; Baumann, K.; Morschhäuser, J.; Schirmeister, T. *ChemMedChem* **2008**, *3*, 302; (c) Büchold, C.; Hemberger, Y.; Heindl, C.; Welker, A.; Degel, B.; Pfeuffer, T.; Staib, P.; Schneider, S.; Rosenthal, P. J.; Gut, J.; Morschhäuser, J.; Bringmann, G.; Schirmeister, T. *ChemMedChem* **2011**, *6*, 141.
11. Korting, H. C.; Schaller, M.; Eder, G.; Hamm, G.; Böhmer, U.; Hube, B. *Antimicrob. Agents Chemother.* **1999**, *43*, 2038.
12. Abad-Zapatero, C.; Goldman, R.; Muchmore, S. W.; Hutchins, C.; Stewart, K.; Navaza, J.; Payne, C. D.; Ray, T. L. *Protein Sci.* **1996**, *5*, 640.
13. (a) Pichova, I.; Pavlickova, L.; Dostal, J.; Dolejsi, E.; Hruskova-Heidingsfeldova, O.; Weber, J.; Ruml, T.; Soucek, M. *Eur. J. Biochem.* **2001**, *268*, 2669; (b) Backman, D.; Danielson, U. H. *Biochim. Biophys. Acta, Proteins Proteomics* **2003**, *1646*, 184; (c) Tossi, A.; Benedetti, F.; Norbedo, S.; Skrbec, D.; Berti, F.; Romeo, D. *Bioorg. Med. Chem.* **2003**, *11*, 4719.
14. (a) Abad-Zapatero, C.; Goldman, R.; Muchmore, S. W.; Hutchins, C.; Oie, T.; Stewart, K.; Cutfield, S. M.; Cutfield, J. F.; Foundling, S. I.; Ray, T. L. *Adv. Exp. Med. Biol.* **1998**, *436*, 297; (b) Sanglard, D.; Odds, F. C. *Lancet Infect. Dis.* **2002**, *2*, 73; (c) Peres-Bota, D.; Rodriguez-Villalobos, H.; Dimopoulos, G.; Melot, C.; Vincent, J. L. *Clin. Microbiol. Infect.* **2004**, *10*, 550.
15. Trabocchi, A.; Mannino, C.; Machetti, F.; De Bernardis, F.; Arancia, S.; Cauda, R.; Cassone, A.; Guarna, A. *J. Med. Chem.* **2010**, *53*, 2502.
16. Morris, G. M.; Goodsell, D. S.; Halliday, R. S.; Huey, R.; Hart, W. E.; Belew, R. K.; Olson, A. J. *J. Comput. Chem.* **1998**, *19*, 1639.
17. Mohamadi, F.; Richards, N. G. J.; Guida, W. C.; Liskamp, R.; Lipton, M.; Caufield, C.; Chang, G.; Hendrickson, T.; Still, W. C. *J. Comput. Chem.* **1990**, *11*, 440.
18. Jennings, W. B.; Farrell, B. M.; Malone, J. F. *Acc. Chem. Res.* **2001**, *34*, 885.
19. The key requirement in correctly addressing the hydrogen-bonding interaction with Gly85 for inhibition potency was also demonstrated with poor inhibiton data of parent compounds of hit **1** lacking the carbonyl group at position 2 of the scaffold or possessing a benzoyl group rather than a benzyl moiety at N-3 position of the bicyclic scaffold; see Ref. 15.
20. Cutfield, S. M.; Dodson, E. J.; Anderson, B. F.; Moody, P. C.; Marshall, C. J.; Sullivan, P. A.; Cutfield, J. F. *Structure* **1995**, *3*, 1261.
21. (a) De Bernardis, F.; Sullivan, P. A.; Cassone, A. *Med. Mycol.* **2001**, *39*, 303; (b) De Bernardis, F.; Arancia, S.; Morelli, L.; Hube, B.; Sanglard, D.; Schäfer, W.; Cassone, A. *J. Infect. Dis.* **1999**, *179*, 201.
22. Gillet, A.; Sanner, M.; Stoffler, D.; Olson, A. *Structure* **2005**, *13*, 483.
23. DeLano, W. L. 'The PyMOL Molecular Graphics System.' DeLano Scientific LLC, San Carlos, CA, USA. [http://www.pymol.org.]
24. Jorgensen, W. L.; Tirado-Rives, J. *J. Am. Chem. Soc.* **1988**, *110*, 1657.
25. Still, W. C.; Tempczyk, A.; Hawley, R. C.; Hendrickson, T. *J. Am. Chem. Soc.* **1990**, *112*, 6127.